Inorganic Chemistry

Article

pubs.acs.org/IC

# Mechanism of NO Photodissociation in Photolabile Manganese–NO Complexes with Pentadentate N5 Ligands

Anna C. Merkle,[†] Nicole L. Fry,[‡] Pradip K. Mascharak,*[,‡] and Nicolai Lehnert*[,†]

[†]Department of Chemistry, University of Michigan, 930 North University Avenue, Ann Arbor, Michigan 48109-1055, United States

[‡]Department of Chemistry and Biochemistry, University of California, Santa Cruz, California 95064, United States

Supporting Information

**ABSTRACT:** The Mn-nitrosyl complexes $[Mn(PaPy_3)(NO)](ClO_4)$ (**1**; $PaPy_3^-$ = *N*,*N*-bis(2-pyridylmethyl)amine-*N*-ethyl-2-pyridine-2-carboxamide) and $[Mn(PaPy_2Q)(NO)](ClO_4)$ (**2**, $PaPy_2Q^-$ = *N*,*N*-bis(2-pyridylmethyl)amine-*N*-ethyl-2-quinoline-2-carboxamide) show a remarkable photolability of the NO ligand upon irradiation of the complexes with UV–vis–NIR light [Eroy-Reveles, A. A.; Leung, Y.; Beavers, C. M.; Olmstead, M. M.; Mascharak, P. K. *J. Am. Chem. Soc.* **2008**, *130*, 4447]. Here we report detailed spectroscopic and theoretical studies on complexes **1** and **2** that provide key insight into the mechanism of NO photolabilization in these compounds. IR- and FT-Raman spectroscopy show N–O and Mn–NO stretching frequencies in the 1720–1750 and 630–650 $cm^{-1}$ range, respectively, for these Mn-nitrosyls. The latter value for $\nu$(Mn–NO) is one of the highest transition-metal–NO stretching frequencies reported to this date, indicating that the Mn–NO bond is very strong in these complexes. The electronic structure of **1** and **2** is best described as Mn(I)–$NO^+$, where the Mn(I) center is in the diamagnetic low-spin state and the $NO^+$ ligand forms two very strong $\pi$ backbonds with the $d_{xz}$ and $d_{yz}$ orbitals of the metal. This explains the very strong Mn–NO bonds observed in these complexes, which even supersede the strengths of the Fe– and Ru–NO bonds in analogous (isoelectronic) Fe/Ru(II)–$NO^+$ complexes. Using time-dependent density functional theory (TD-DFT) calculations, we were able to assign the electronic spectra of **1** and **2**, and to gain key insight into the mechanism of NO photorelease in these complexes. Upon irradiation in the UV region, NO is released because of the direct excitation of $d_\pi$_$\pi^*$ → $\pi^*$_$d_\pi$ charge transfer (CT) states (*direct mechanism*), which is similar to analogous NO adducts of Ru(III) and Fe(III) complexes. These are transitions from the Mn–NO bonding ($d_\pi$_$\pi^*$) into the Mn–NO antibonding ($\pi^*$_$d_\pi$) orbitals within the Mn–NO $\pi$ backbond. Since these transitions lead to the population of Mn–NO antibonding orbitals, they promote the photorelease of NO. In the case of **1** and **2**, further transitions with distinct $d_\pi$_$\pi^*$ → $\pi^*$_$d_\pi$ CT character are observed in the 450–500 nm spectral range, again promoting photorelease of NO. This is confirmed by resonance Raman spectroscopy, showing strong resonance enhancement of the Mn–NO stretch at 450–500 nm excitation. The extraordinary photolability of the Mn-nitrosyls upon irradiation in the vis–NIR region is due to the presence of low-lying $d_{xy}$ → $\pi^*$_$d_\pi$ singlet and triplet excited states. These have zero oscillator strengths, but can be populated by initial excitation into $d_{xy}$ → L(Py/Q_$\pi^*$) CT transitions between Mn and the coligand, followed by interconversion into the $d_{xy}$ → $\pi^*$_$d_\pi$ singlet excited states. These show strong spin–orbit coupling with the analogous $d_{xy}$ → $\pi^*$_$d_\pi$ triplet excited states, which promotes intersystem crossing. TD-DFT shows that the $d_{xy}$ → $\pi^*$_$d_\pi$ triplet excited states are indeed found at very low energy. These states are strongly Mn–NO antibonding in nature, and hence, promote dissociation of the NO ligand (*indirect mechanism*). The Mn-nitrosyls therefore show the long sought-after potential for easy tunability of the NO photorelease properties by simple changes in the coligand.

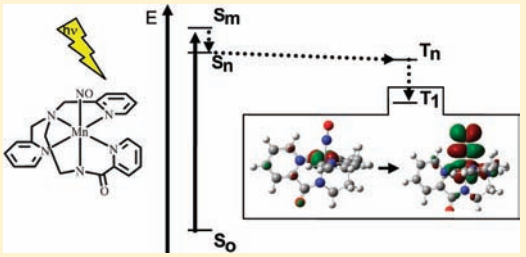


## A. INTRODUCTION

During the past few decades the role of nitric oxide (NO) in several biological functions such as regulation of blood pressure[1] and neurotransmission[2] has been firmly established.[3] These processes require low concentrations (nM) of endogenous NO that is produced from L-arginine by the enzyme nitric oxide synthase (NOS). In addition, macrophages use relatively high concentrations ($\mu$M) of NO to fight invading pathogens as part of our innate immune system.[4] Interestingly, studies have shown that exogenous NO can also be used to induce similar biological responses[5,6] as well as other pathological outcomes. For example, it has been shown that high fluxes of NO can lead to apoptosis in malignant cells of different grade and origin.[7,8] This finding has prompted research aimed at developing suitable NO donors for the treatment of cancer.[9,10]

Metal-nitrosyls that release large quantities of NO upon light exposure would be ideal for site specific delivery of NO to malignant locations.[11,12] Such treatment will come under the realm of Photodynamic Therapy (PDT).[13,14] Historically, the bulk of research on photolabile metal-nitrosyls involved iron-[15]

**Received:** September 7, 2011
**Published:** October 31, 2011

and ruthenium-nitrosyls.[16] Studies in this area have indicated that although iron-nitrosyls tend to be more sensitive to low-energy visible light releasing large amounts of NO, the complexes in general tend to be less stable in aqueous environment. Conversely, most ruthenium-nitrosyls are more stable in aqueous media but require UV light for NO release. This trend becomes clear upon comparison of two isoelectronic iron- and ruthenium-nitrosyls, $[Fe(PaPy_3)(NO)](ClO_4)_2$ and $[Ru(PaPy_3)(NO)](BF_4)_2$, ($PaPy_3^-$ = *N*,*N*-bis(2-pyridylmethyl)amine-*N*-ethyl-2-pyridine-2-carboxamide) reported by us previously.[17,18] When exposed to visible light (500−600 nm), $[Fe(PaPy_3)(NO)](ClO_4)_2$ releases NO with a quantum yield ($\phi$) of 0.18[17,19] while $[Ru(PaPy_3)(NO)](BF_4)_2$ requires UV light (300−450 nm) for NO release and exhibits a lower quantum yield ($\phi \sim 0.05$).[18,20] Since UV light is inherently detrimental to cellular targets, we looked into the possibility of the use of other metal-nitrosyls in light-triggered NO release. Interestingly, the manganese-nitrosyl $[Mn(PaPy_3)(NO)](ClO_4)$ (**1**) not only releases NO upon exposure to low-energy *visible* (500−600 nm) light but also exhibits stability in aqueous media.[21] We have been able to further enhance this sensitivity to even lower energy light (500−800 nm) by replacing one pyridine ring of the $PaPy_3^-$ ligand frame with a quinoline moiety (cf. Scheme 1) in the resulting manganese

**Scheme 1**

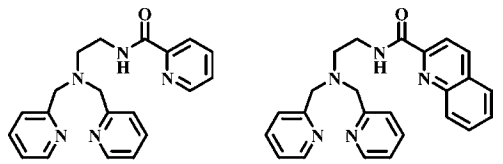


nitrosyl $[Mn(PaPy_2Q)(NO)](ClO_4)$ (**2**, $PaPy_2Q^-$ = *N*,*N*-bis(2-pyridylmethyl)amine-*N*-ethyl-2-quinoline-2-carboxamide).[21]

Currently there are relatively few manganese-nitrosyls reported in the literature and even fewer studies that examine their electronic structures in detail. The favorable properties of **1** and **2** have prompted us to further examine their electronic structures to gain insights into structure−function relationships leading to NO labilization with *low-energy* light. Such studies are necessary for the smart design of nitrosyls with improved NO donating ability. The noninnocent nature of the NO ligand (possibility of existing as $NO^+$, $NO^\bullet$, or $NO^-$ in metal-nitrosyl complexes) in general poses a problem in the correct assignment of the formal oxidation states of the metal centers in nitrosyl complexes.[22] Both **1** and **2** are diamagnetic Mn(II) complexes with NO, {Mn−NO}$^6$ in the Enemark−Feltham notation,[23] and hence there are three possible electronic descriptions: Mn(I)−$NO^+$, Mn(II)−NO(radical), or Mn(III)−$NO^-$. In earlier work, researchers have suggested formal oxidation states based on the metric parameters of the Mn−N−O unit. For example, a low-spin Mn(I)−$NO^+$ formulation has been suggested for the diamagnetic {Mn−NO}$^6$ complexes [Mn(TPP)(NO)] ($TPP^{2-}$ = tetraphenylporphinato dianion)[24] and [Mn-(5-$CH_3$SALDPT)(NO)] (SALDPT = dianionic pentadentate Schiff base ligand).[25] These complexes have similar NO stretching frequencies ($\nu$(N−O) = 1735 and 1715 $cm^{-1}$, respectively) compared with those of **1** (1733 $cm^{-1}$) and **2** (1725 $cm^{-1}$), indicating similar electronic descriptions. However, more recently Lippard and Ghosh have used density functional theory (DFT) calculations[26] in addition to magnetic and spectroscopic data to assign the paramagnetic tropocoronand complex, [Mn(NO)(TC-5,5)], as a Mn(III)−$NO^-$ species.[27] Interestingly, the Mn−N−O angle and Mn−N/N−O bond distances of [Mn(NO)(TC-5,5)] (174.1(3)°, 1.699(3) and 1.179(3) Å, respectively) are very similar to those of [Mn(TPP)(NO)] (174.9(6)°, 1.644(5) and 1.176(7) Å, respectively). Clearly, the use of metric data alone is not enough to correctly assign the oxidation states of the metal centers in such nitrosyls.

In this study, the spectroscopic properties and the electronic structures of **1** and **2** are investigated using UV−vis absorption, IR, and resonance Raman spectroscopy coupled to DFT calculations. Raman spectra of the nitrosyl complex **1** are presented for the first time. Using $^{15}N^{18}O$ isotope substitution, the IR and Raman spectra of **1** are assigned, including N−O and Mn−NO stretching and Mn−N−O bending vibrations. Compared to DFT calculations on both singlet and triplet states, such measurements allow for an unambiguous definition of the ground state of these complexes and the formal oxidation states of Mn and NO in **1** and **2**. From these calculations, the electronic structure of both complexes has been defined, and the properties of nitric oxide as a ligand have been evaluated. Finally, details of the photochemistry of **1** and **2** are reported. Time-dependent DFT (TD-DFT) calculations are used to assign the visible absorption spectra of **1** and **2**, and to gain insight into the photophysical mechanisms of NO dissociation in these compounds.

## B. EXPERIMENTAL AND COMPUTATIONAL PROCEDURES

**Syntheses of Compounds.** (UC Santa Cruz and University of Michigan) The ligands *N*,*N*-bis(2-pyridylmethyl)amine-*N*-ethyl-2-pyridine-2-carboxamide ($PaPy_3H$) and *N*,*N*-bis(2-pyridylmethyl)-amine-*N*-ethyl-2-quinoline-carboxamide ($PaPy_2QH$), and the corresponding Mn-nitrosyls, $[Mn(PaPy_3)(NO)]ClO_4$ and $[Mn(PaPy_2Q)(NO)]ClO_4$, respectively, were all synthesized according to literature procedures.[28,29] The starting material, $[Mn(PaPy_3)(H_2O)]ClO_4$, was also synthesized according to previously published methods.[21] Nitric oxide (Cryogenic Gases, Detroit, MI) was purified by first passing through an ascarite II column (NaOH on silica gel) and then through a cold trap at −80 °C to exclude higher nitrogen oxide impurities. Isotopically labeled $^{15}N^{18}O$ was purchased from Sigma-Aldrich and was used as received. All solvents were dried by standard techniques and distilled prior to use. Standard Schlenk techniques were used during all syntheses.

**Vibrational Spectroscopy.** (University of Michigan) FT-Raman spectra were recorded on a Bruker IFS 66 interferometer with a Bruker FRA 106 Raman attachment using a Nd:YAG laser for excitation ($\lambda$ = 1064 nm). Measurements were performed on pure compounds. The resolution was set to 2 $cm^{-1}$. Mid-infrared (MIR) spectra were obtained from KBr disks on a Perkin-Elmer FT-IR spectrometer SPECTRUM Bx.

The resonance Raman (rRaman) spectra were obtained on frozen solutions of $[Mn(PaPy_3)(NO)]ClO_4$ and the corresponding $^{15}N^{18}O$ labeled complex in $CH_3CN$ using 413, 457, 472, 488, 514, and 647 nm excitation from a SpectraPhysics Beamlok 2060-RS $Kr^+/Ar^+$ ion gas laser. The excitation beam (10−20 mW) was focused onto a ~10.5 mM sample in an electron paramagnetic resonance (EPR) tube contained in an EPR coldfinger dewar with liquid $N_2$ to prevent thermal degradation and photolabilization. The scattered photons were dispersed by an Acton two-stage TriVista 555 monochromator and detected by a liquid $N_2$-cooled Princeton Instruments Spec-10:400B/LN CCD camera. A typical resolution in these experiments was 0.5 $cm^{-1}$.


dx.doi.org/10.1021/ic201967f | Inorg. Chem. 2011, 50, 12192−12203

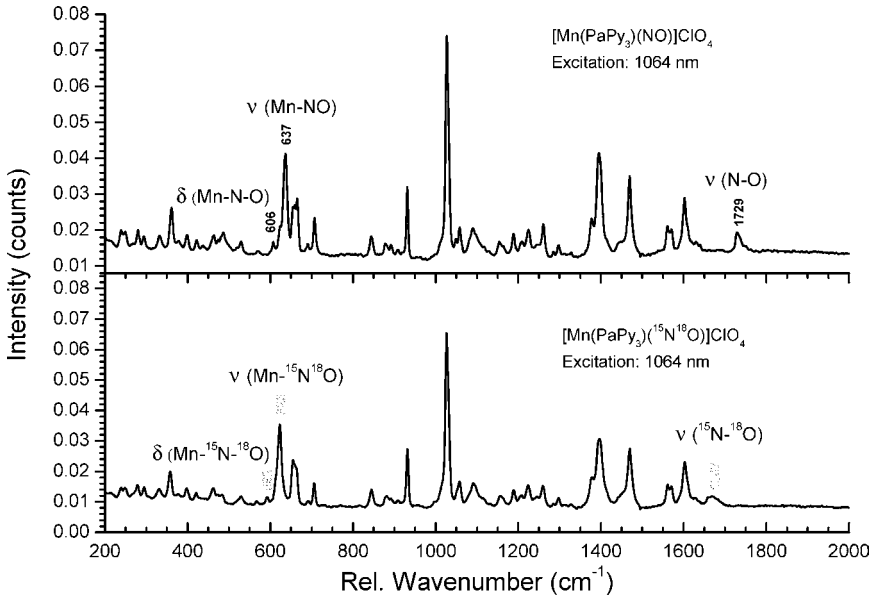


**Figure 1.** FT-Raman spectra of $[Mn(PaPy_3)(NO)]^+$ (top) and $[Mn(PaPy_3)(^{15}N^{18}O)]^+$ (bottom), excited at 1064 nm.

**Table 1. Experimental and Computational Vibrational Data of $[Mn(PaPy_3)(NO)]^+$ and $[Mn(PaPy_2Q)(NO)]^+$**

| | experimental [$cm^{-1}$][a] | | | | DFT: BP86/TZVP [$cm^{-1}$], $S$ =0 | | | |
|---|---|---|---|---|---|---|---|---|
| complex | $\nu$(N−O) | $\nu$(Mn−NO) | $\delta$(Mn−N−O) | $\nu$(C=O) | $\nu$(N−O) | $\nu$(Mn−NO) | $\delta$(Mn−N−O) | $\nu$(C=O) |
| $[Mn(PaPy_3)(NO)]^+$ | 1733 (IR) 1729 (R) | 637 (R)[c] | 606 (R) | 1630 (IR) | 1758 | 653 | 613/631 | 1649 |
| $[Mn(PaPy_3)(^{15}N^{18}O)]^+$ | 1664 (IR) 1667 (R) | 623 (R) | 592 (R) | 1630 (IR) | 1684 | 638 | 620/597 | 1649 |
| Difference (N.A.I.-$^{15}N^{18}O$)[b] | 69 (IR) 60 (R) | 14 | 14 | 0 | 74 | 15 | 10/15 | 0 |
| $[Mn(PaPy_2Q)(NO)]^+$ | 1725 (IR) | | | 1634 | 1737 | 669 | 612/630 | 1641 |

[a]R = Raman spectroscopy. [b]N.A.I. = natural abundance isotopes complex. [c]Observed at 637 $cm^{-1}$ in the solid and at 639 $cm^{-1}$ in frozen solution (cf. Figures 1 and 2, respectively).

**DFT Calculations.** (University of Michigan) The structures of $[Mn(PaPy_3)(NO)]^+$ and $[Mn(PaPy_2Q)(NO)]^+$ were fully optimized (for both $S$ = 0, 1 states) without simplifications applying the BP86 functional[30,31] together with Ahlrichs' TZVP basis set.[32,33] The vibrational frequencies of the fully optimized complexes were again calculated with BP86/TZVP, showing no imaginary frequencies. IR and non-resonance Raman intensities were calculated as well to assist in spectral assignments. All of these calculations were performed using Gaussian 03.[34] To calculate the absorption spectrum of $[Mn(PaPy_3)(NO)]^+$, the TD-DFT formalism was applied using both BP86/TZVP and B3LYP/TZVP. Since BP86/TZVP gave an overall better agreement with experiment in the important visible region of the spectrum (see Supporting Information, Figure S1), this method was used to further assign the UV−vis absorption spectrum of **1**. TD-DFT calculations were performed using ORCA (University of Bonn).[35] Orbitals were plotted with the program GaussView.

## C. RESULTS AND ANALYSIS

**C.1. Spectroscopic and Physical Properties.** *Synthesis and Electrochemistry.* Both nitrosyls **1** and **2** were synthesized from their respective water-bound complexes $[Mn(PaPy_3)(H_2O)](ClO_4)$ (**3**) and $[Mn(PaPy_2Q)(H_2O)](ClO_4)$ (**4**). A strong EPR signal with $g$ = 2.00 confirms **3** as a low spin ($S$ = 1/2) Mn(II) species.[21] Conversely, room-temperature EPR measurements indicate that **4** contains a high-spin ($S$ = 5/2) Mn(II) center.[29] Upon exposure to NO gas, the water ligand in **3** and **4** is replaced with NO resulting in the formation of the $\{MnNO\}^6$ nitrosyls **1** and **2**. Room temperature magnetic susceptibility data and sharp resonances in the $^1$H NMR spectra of both complexes indicate that these compounds are diamagnetic ($S$ = 0) in the solid state and in solution. Electrochemical studies using cyclic voltammetry (CV) on **1** and **2** do not show any reduction of either complex at potentials as low as −1.0 V vs SCE.[21,29] However, both nitrosyls exhibit quasireversible oxidation processes with $E_{1/2}$ = 0.9 V vs SCE. In the case of **1**, the oxidized product was isolated as $[Mn(PaPy_3)(NO)](NO_3)_2$ ($\mathbf{1}^{ox}$).[21,36]

*Vibrational Properties.* The IR spectra of both **1** and **2** contain strong N−O stretching frequencies, $\nu$(N−O), at 1733 $cm^{-1}$ and 1725 $cm^{-1}$, respectively. Upon $^{15}N^{18}O$ isotope labeling, $\nu$(N−O) of **1** shifts to 1664 $cm^{-1}$, which confirms this assignment. To determine the energies of the Mn−NO stretching and Mn−N−O (linear) bending modes, $\nu$(Mn−NO) and $\delta$(Mn−N−O), Raman spectroscopy was applied. Figure 1 shows the non-resonance FT-Raman spectrum of **1** and of the corresponding $^{15}N^{18}O$ isotope labeled complex. From these data, two isotope-sensitive features are readily identified at 637 $cm^{-1}$ and 606 $cm^{-1}$, which shift to 623 $cm^{-1}$ and 592 $cm^{-1}$, respectively, in the $^{15}N^{18}O$ compound (cf. Table 1). We assign the higher energy feature to the Mn−NO stretch based on three observations. First, the 637 $cm^{-1}$ feature shows significantly higher intensity in the Raman spectrum compared to the 606 $cm^{-1}$ band, which is in agreement with previous assignments of the Ru−NO stretching and Ru−N−O bending modes in $[Ru(NH_3)_5(NO)]X_3$, where the stretch showed considerably more intensity in the FT-Raman spectrum than the bend.[37] Second, the 637 $cm^{-1}$ feature shows resonance enhancement upon laser excitation in the visible region as


dx.doi.org/10.1021/ic201967f | Inorg. Chem. 2011, 50, 12192–12203

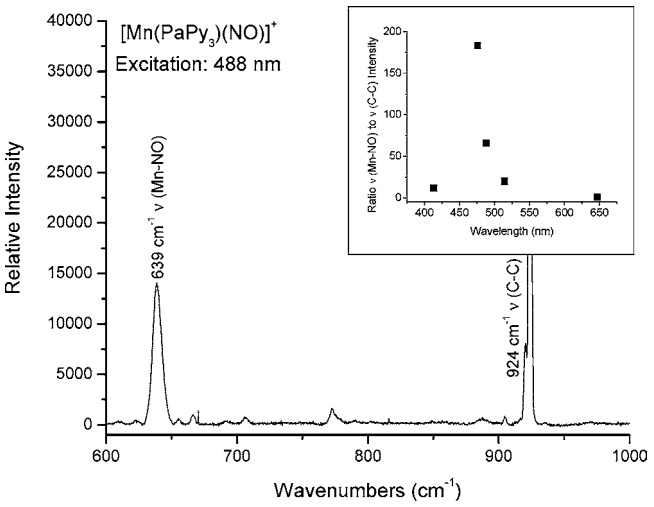


**Figure 2.** Resonance Raman spectrum of $[Mn(PaPy_3)(NO)]^+$ obtained at an excitation wavelength of 488 nm. Inset: resonance Raman excitation profile of the 639 $cm^{-1}$ feature, showing resonance enhancement of this vibration toward the UV region. The ratio of $\nu$(Mn−NO) to $\nu$(C−C) (MeCN) Raman intensity is normalized to the value observed at the excitation wavelength of 647 nm (intensity ratio set to 1).

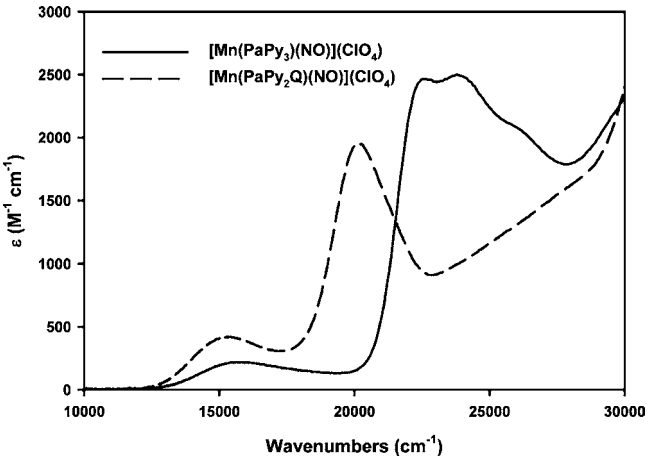


**Figure 3.** Electron absorption spectra of $[Mn(PaPy_3)(NO)]^+$ (solid, black line) and $[Mn(PaPy_2Q)(NO)]^+$ (dashed, black line) obtained in MeCN at room temperature.

shown in Figure 2 (observed at 639 $cm^{-1}$ in frozen solution), whereas the 606 $cm^{-1}$ feature is not observed under these conditions. Resonance Raman enhancement of metal−ligand vibrations is in most cases related to charge-transfer transitions between the metal and the ligand that lead to a change in the metal−ligand bond in the excited state, and in this way, to an excited state displacement, $\Delta Q$.[38−40] These excited state displacements are generally much more pronounced for metal−ligand bond distances compared to angles, and hence, the metal−ligand stretching, but not bending, modes are in most cases resonance enhanced.[41] The fact that the 637 $cm^{-1}$ mode shows strong resonance enhancement (cf. Figure 2, inset) is therefore indicative that this is in fact the Mn−NO stretch. Finally, our DFT calculations (see below) further support this assignment, as they predict $\nu$(Mn−NO) to be at higher energy than $\delta$(Mn−N−O). These assignments are summarized in Table 1. The obtained energy for $\nu$(Mn−NO) also compares well with that reported for NO adducts of Mn-substituted myo- and hemoglobin, observed at ∼625 $cm^{-1}$.[42]

*Electronic Absorption Spectroscopy.* The green MeCN solution of **1** exhibits absorption bands with $\lambda_{max}$ at 22730 (440 nm, $\varepsilon$ = 2460 $M^{-1}$ $cm^{-1}$) and 15750 $cm^{-1}$ (635 nm, $\varepsilon$ = 220 $M^{-1}$ $cm^{-1}$). The additional conjugation provided by replacement of one pyridine donor with a quinoline moiety in the ligand frame of **2** shifts the position of the absorbance bands to lower energy. For example, the maroon solution of **2** in MeCN displays bands with $\lambda_{max}$ at 20200 $cm^{-1}$ (495 nm, $\varepsilon$ = 2030 $M^{-1}$ $cm^{-1}$) and 15385 $cm^{-1}$ (650 nm, $\varepsilon$ = 420 $M^{-1}$ $cm^{-1}$). Interestingly, the extinction coefficient of the low-energy band of **2** is increased to a significant extent as seen in Figure 3. In comparison, in the case of the corresponding Ru-nitrosyls, $[Ru(PaPy_3)(NO)](BF_4)_2$ and $[Ru(PaPy_2Q)(NO)](BF_4)_2$, there is a much smaller red-shift in $\lambda_{max}$ (∼580 $cm^{-1}$) upon addition of the quinoline moiety.[18,20]

*NO Photolability Measurements.* When solutions of **1** and **2** are exposed to visible light of low intensity (5 mW), rapid loss of NO occurs with concomitant formation of the colorless solvent-bound Mn(II) photoproducts, $[Mn(PaPy_3)(Solv)]^{2+}$ or $[Mn(PaPy_2Q)(Solv)]^{2+}$, respectively. No loss of NO is noted when the solutions are kept in the dark for 48 h. The quantum yield values ($\phi$) of **1** and **2** have been determined from changes in the electronic absorption spectra upon exposing the complexes to light of two different wavelengths (500 and 550 nm) in MeCN. The $\phi$ value of **2** (0.623 ± 0.010 and 0.579 ± 0.010 at 500 and 550 nm, respectively) are significantly larger than the values of **1** (0.326 ± 0.010 and 0.309 ± 0.010, respectively). This indicates that incorporation of a quinoline moiety in place of the pyridine group is effective not only in moving the photosensitivity to light of longer wavelengths but also in improving $\phi$ values of the resulting Mn-nitrosyl. The latter effect, that is, the approximate doubling of $\phi$ in complex **2** relative to **1** upon excitation at 500 and 550 nm indicates that **2** has more efficient interconversion channels of the initially excited CT states into the key NO photoreleasing triplet excited states (see Discussion) than **1** (since $\phi$ is normalized to the extinction of the sample). Additional photophysical studies published previously[36] show that complex **2** photolabilizes NO even upon excitation with NIR light (up to 800 nm), which demonstrates that **2** is a superior NO donor compared to **1** for potential applications *in vivo*.

**C.2. Electronic Structure of the Manganese(II) Complexes with NO.** To further investigate the electronic structures of **1** and **2**, and to explain the apparent strength of the Mn−NO bond in these complexes, we applied DFT calculations using the BP86/TZVP functional/basis set combination that has proven to deliver good structures for transition-metal nitrosyls in the past.[22,43−50] The structures of the two complexes $[Mn(PaPy_3)(NO)]^+$ and $[Mn(PaPy_2Q)(NO)]^+$ were optimized without simplifications for both $S$ = 0 and $S$ = 1 as potential ground states. Figure 4 shows the obtained structures for the $S$ = 0 cases, and calculated geometric parameters are compared to experiment in Table 2. As can be seen from these data, excellent agreement is obtained between the experimental and DFT-calculated structures for the $S$ = 0 state. The predicted vibrational data for the $S$ = 0 and $S$ = 1 states are listed in Table 3. The calculated vibrational frequencies provide further support for the idea that both **1** and **2** have diamagnetic ($S$ = 0) ground states. Interestingly, the N−O stretching frequency is quite insensitive to this change in spin state, and is predicted, for


dx.doi.org/10.1021/ic201967f | Inorg. Chem. 2011, 50, 12192−12203

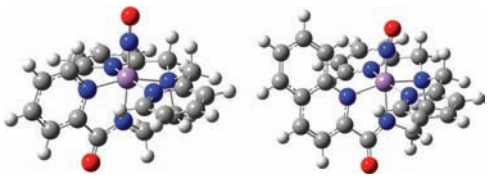

**Figure 4.** Fully optimized structures of $[Mn(PaPy_3)(NO)]^+$ (left) and $[Mn(PaPy_2Q)(NO)]^+$ (right) for $S = 0$, obtained with BP86/TZVP. Structural data are given in Table 2.

example, at 1758 versus 1761 $cm^{-1}$ in the singlet and triplet state of **1**, respectively. In contrast, the Mn−NO stretch and the Mn−N−O linear bend are very sensitive to the difference in spin state, and are predicted to shift about 70−80 $cm^{-1}$ to lower frequency in the triplet state as shown in Table 3. On the basis of this comparison, it can be safely concluded that both **1** and **2** have diamagnetic ($S = 0$) ground states. The predicted energy difference between the $S = 0$ and $S = 1$ states of **1** and **2** is 16 and 14 kcal/mol, respectively, again favoring the ground state to be $S = 0$.

On the basis of the exceptional agreement between the optimized and experimental structures of **1** and **2**, we then used the optimized structure of **1** to further characterize the electronic structures of these manganese-nitrosyls in their $S = 0$ ground states. Figure 5 shows the calculated MO diagram of $[Mn(PaPy_3)(NO)]^+$. In this complex, the Mn(II) ion is in the low-spin state, which would lead to a $[t_{2g}]^5$ electron configuration. However, the additional (unpaired) electron of NO is used to fill the remaining hole in the $t_{2g}$ shell, leading to a formally Mn(I) center with a $[t_{2g}]^6$ electron configuration, and a bound $NO^+$ ligand. Hence, the ground state is represented by a closed-shell electron configuration, $S = 0$, where all electrons are perfectly paired. As shown in Figure 5, the highest occupied molecular orbital (HOMO) of **1** is the $d_{xy}$ orbital (MO <110>), which is nonbonding with respect to the $NO^+$ ligand. Here, we apply a coordinate system where the Mn−N(O) bond corresponds to the $z$ axis. An iso-density surface plot of MO <110>, corresponding to the $d_{xy}$ orbital of Mn, is shown in Figure 6. Note that simplified ChemDraw representations of important MOs are also included in Figure 5, right, to further illustrate the properties of these orbitals with respect to metal−ligand interactions. To lower energy, two $PaPy_3^-$ ligand-based orbitals are found, MO <109> and MO <108>, followed by the two bonding combinations between the $\pi^*$ orbitals of the formally $NO^+$ unit and the $d_{xz}$ and $d_{yz}$ orbitals of the metal, labeled $d_{xz}\_\pi_x^*$ (MO <107>) and $d_{yz}\_\pi_y^*$ (MO <106>). The corresponding antibonding combinations, $\pi_x^*\_d_{xz}$ (MO <113>) and $\pi_y^*\_d_{yz}$ (MO <115>), are unoccupied and found to be slightly higher energy than the lowest unoccupied molecular orbital (LUMO) of the complex. Iso-density surface plots of all of these key orbitals are shown in Figure 6, and Figure 5 includes simplified ChemDraw representations of these MOs. The LUMO and LUMO+1 of **1** are $PaPy_3^-$ ligand-based MOs, centered on the pyridine rings (MOs <111/112>; cf. Figure 5). As shown in Figure 6, the $d_{yz}\_\pi_y^*$ bonding combination also shows strong admixture of the $p_y$ donor orbital of the amide nitrogen atom of $PaPy_3^-$, trans to NO, which is located at similar energy as the $t_{2g}$ orbitals of manganese. Figure 5 shows ChemDraw representations that better illustrate this interaction. The main component of this amide orbital is observed in MO <109> (cf. Figure 6), which has 55% amide character. On the other hand, the $\pi_y^*\_d_{yz}$ antibonding combination is mixed with pyridine $\pi^*$ orbitals (see MO <115> in Figure 6). Because of this complication, the strength of the Mn(I)−$NO^+$ $\pi$ backbond is best estimated from the $d_{xz}/\pi_x^*$ set: here, the occupied MO, $d_{xz}\_\pi_x^*$ (MO <107>), has 54% Mn and 36% $NO^+$ character, whereas the antibonding combination, $\pi_x^*\_d_{xz}$ (MO <113>), has 54% $NO^+$ and 37% Mn contributions (see also the simplified drawings of these MOs in Figure 5). The fact that the occupied MO has more metal character is again in agreement with the idea that these electrons should formally be assigned to manganese, in accordance with the Mn(I)−$NO^+$ description. Nevertheless, these charge contributions correspond to an extraordinarily strong $\pi$ backbond, because of the soft nature of the formally

**Table 2. Structural Data of $[Mn(PaPy_3)(NO)]^+$ and $[Mn(PaPy_2Q)(NO)]^+$ from X-ray Crystallography[21,29] and DFT Calculations (BP86/TZVP)**

| | $[Mn(PaPy_3)(NO)]^+$ | | $[Mn(PaPy_2Q)(NO)]^+$ | |
|---|---|---|---|---|
| | crystal structure | DFT calculation ($S = 0$) | crystal structure | DFT calculation ($S = 0$) |
| Mn−NO [Å] | 1.66 | 1.67 | 1.68 | 1.67 |
| N−O [Å] | 1.19 | 1.18 | 1.21 | 1.19 |
| Mn−N−O [deg] | 172° | 180° | 165° | 169° |
| $Mn-N_{amide}$ [Å] | 1.96 | 1.96 | 1.96 | 1.96 |
| $Mn-N_{amine}$ [Å] | 2.03 | 2.06 | 2.06 | 2.06 |
| $Mn-N_{py(trans\ amide)}$ [Å] | 2.00 | 2.00 | 2.09 | 2.06 |
| $Mn-N_{py(trans\ py)}$ [Å] | 2.03, 2.02 | 2.05, 2.05 | 2.06, 2.03 | 2.04, 2.05 |

**Table 3. Comparison of Key Calculated Vibrational Data (BP86/TZVP) of the Potential $S = 0$ and $S = 1$ Ground States of $[Mn(PaPy_3)(NO)]^+$ and $[Mn(PaPy_2Q)(NO)]^+$**

| complex | vibrations | singlet: $S = 0$ | triplet: $S = 1$ | experimental |
|---|---|---|---|---|
| $[Mn(PaPy_3)(NO)]^+$ | $\nu$(N−O) | 1758 $cm^{-1}$ | 1761 $cm^{-1}$ | 1733 $cm^{-1}$ |
| | $\nu$(Mn−NO) | 653 $cm^{-1}$ | 582 $cm^{-1}$ | 637 $cm^{-1}$ |
| | $\delta$(Mn−N−O) | 613/631 $cm^{-1}$ | 520/550 $cm^{-1}$ | 606 $cm^{-1}$ |
| $[Mn(PaPy_2Q)(NO)]^+$ | $\nu$(N−O) | 1737 $cm^{-1}$ | 1746 $cm^{-1}$ | 1725 $cm^{-1}$ |
| | $\nu$(Mn−NO) | 669 $cm^{-1}$ | 590 $cm^{-1}$ | |
| | $\delta$(Mn−N−O) | 612/630 $cm^{-1}$ | 525/551 $cm^{-1}$ | |


dx.doi.org/10.1021/ic201967f | Inorg. Chem. 2011, 50, 12192–12203

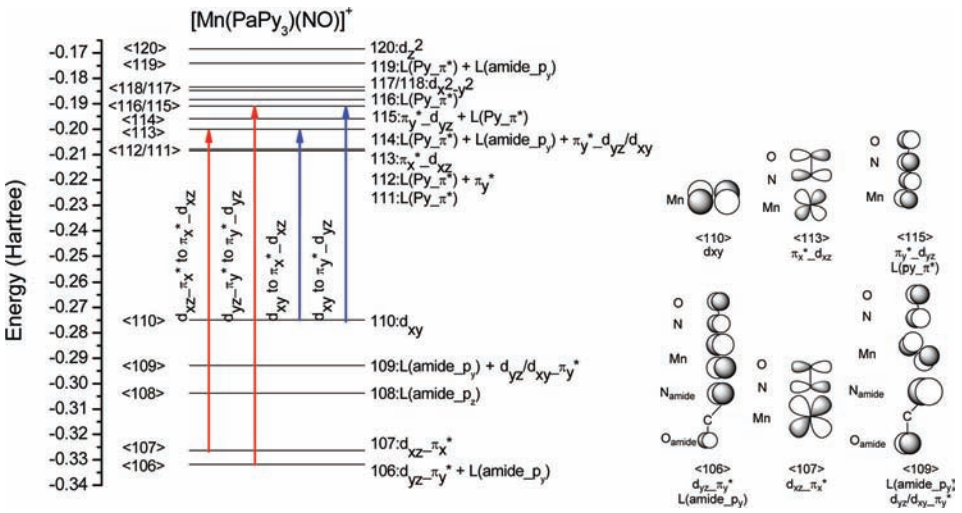


**Figure 5.** MO diagram of $[Mn(PaPy_3)(NO)]^+$ ($S = 0$) calculated with BP86/TZVP. In the applied coordinate system, the $z$ axis points along the Mn−N(O) bond. The nomenclature "*a_b*" indicates that orbital *a* interacts with *b* and that *a* has a larger contribution to the resulting MO. Contour plots of important MOs are provided in Figure 6. Symmetry-allowed (red arrows) and -forbidden (blue arrows) MLCT transitions are indicated (see text). On the right, ChemDraw representations of key MOs are included.

Mn(I) center. Hence, via covalency (orbital mixing), the charge density of about 1.3 electrons is transferred back from the Mn(I) center to $NO^+$. Since the transferred charge density has 50% $\alpha$ and 50% $\beta$ spin, this does *not* correspond to an electron transfer, because an electron has a charge *and* a corresponding spin. This is purely an effect of metal−ligand covalency. Finally, the $\sigma$ bond between Mn(I) and $NO^+$ is weak: as shown in Figure 6, the corresponding antibonding combination between $d_{z^2}$ and the $\sigma$-donor orbital of $NO^+$, MO <120>, only has 7% NO character. Therefore, the Mn(I)−$NO^+$ interaction in **1** is dominated by $\pi$ backbonding.

The electronic structure of the optimized triplet complex mentioned above corresponds to a $[d_{xz}^2 d_{yz}^2 d_{xy}^1 d_{x^2-y^2}^1]$ electron configuration, that is, a $d_{xy} \rightarrow d_{x^2-y^2}$ ligand field (excited) triplet state relative to the singlet ground state. Here, the triplet electron configuration leads to a strong spin polarization of the Mn−NO backbond. In fact, the complex adopts an electronic structure that is now better described as Mn(III)−$NO^-$. In the case of the $\alpha$-MOs, the Mn−NO backbond is greatly weakened compared to the singlet ground state, whereas in the $\beta$-MO case, an inverted bonding scheme is observed where the occupied orbitals of the Mn−NO $\pi$ bond now have more dominant $\pi^*$(NO) character. Hence, NO can be considered as $NO^-$ ($S = 1$) ligand where both $\beta$−$\pi^*$ orbitals of NO are singly occupied and strongly donate into the $\beta$-$d_{xz}$ and $\beta$-$d_{yz}$ orbitals of Mn (in the coordinate system applied here). This situation is similar to ferrous nonheme iron-nitrosyls.[51] This leads to a less covalent, weaker Mn−NO bond compared to the singlet ground state, which explains the predicted reduction of the Mn−NO stretching frequency from 653 (for $S = 0$) to 582 $cm^{-1}$ (for $S = 1$) in the calculation for **1**. Collectively, these theoretical results along with the resonance Raman data strongly suggest that the Mn(III)−$NO^-$ description is not appropriate for the ground states of the present set of manganese-nitrosyls.

The MO diagram of $[Mn(PaPy_2Q)(NO)]^+$ (not shown) in the singlet ground state is overall similar to $[Mn(PaPy_3)(NO)]^+$, but more complex because of the additional ligand orbitals present in the HOMO−LUMO region that originate from the quinoline (Q) group. The small differences between **1** and **2** in terms of electronic structure are directly reflected by

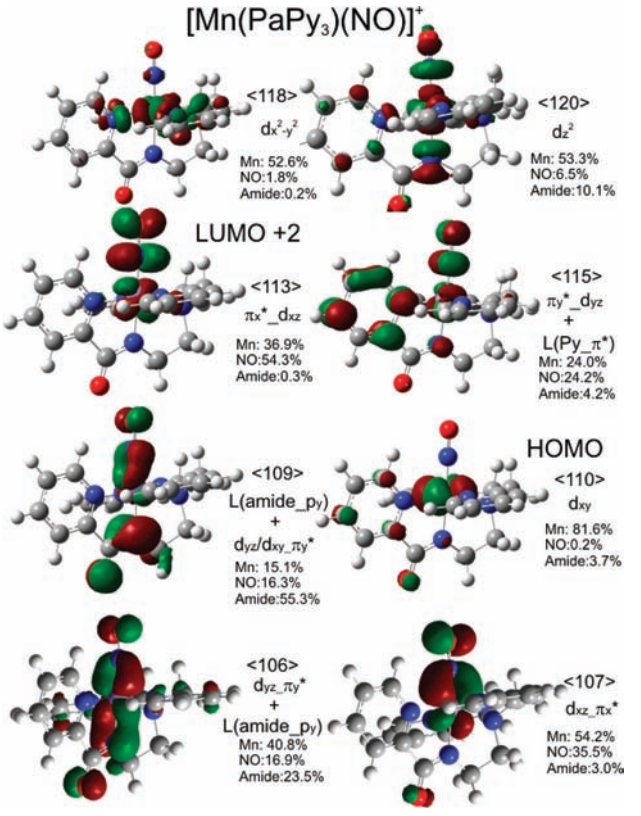


**Figure 6.** Iso-density surface plots of important MOs of $[Mn(PaPy_3)(NO)]^+$, calculated with BP86/TZVP. Orbital energies increase from bottom to top. Percent decompositions of these MOs are included.

the calculated vibrational frequencies, where **1** has a higher $\nu$(N−O) and lower $\nu$(Mn−NO) frequency compared to **2** (cf. Table 3). This inverse correlation of the N−O and metal−NO stretching frequencies between **1** and **2** directly indicates that complex **2** has a *slightly* stronger Mn(I)−$NO^+$ $\pi$ backbond.[52] Here, an increased donation from the $d_\pi$ orbitals of the metal into $\pi^*$ of $NO^+$ leads to a weaker N−O bond (lower $\nu$(N−O)


dx.doi.org/10.1021/ic201967f | Inorg. Chem. 2011, 50, 12192–12203

Table 4. Selected Electronic Transitions in $[Mn(PaPy_3)(NO)]^+$ (1) Calculated with TD-DFT (BP86/TZVP), and Analysis of Underlying One-Electron Transitions

| band | TD-DFT states | energy [$cm^{-1}$] | energy [nm] | $f$(osc) | major contribution[a] | percent contribution |
|---|---|---|---|---|---|---|
| 1 | S4 | 14663 | 682 | 0.002 | $d_{xy}$ to L(Py_$\pi^*$) | 49% |
| 1 | S6 | 15368 | 651 | 0.006 | $d_{xy}$ to L(Py_$\pi^*$) | 42% |
| 2 | S13 | 18716 | 534 | 0.006 | $d_{yz}/d_{xy}$_$\pi_y^*$ to L(Py_$\pi^*$)<br>L(amide_$p_y$) to L(Py_$\pi^*$) | 45% |
| 2 | S15 | 18881 | 530 | 0.006 | $d_{xy}$ to L(Py_$\pi^*$) | 31% |
| 3 | S31 | 21945 | 456 | 0.031 | $d_{xy}$ to L(Py_$\pi^*$) | 30% |
| 4 | S38 | 23315 | 429 | 0.012 | $d_{xy}$ to L(Py_$\pi^*$) | 23% |
| 4 | S42 | 24059 | 416 | 0.017 | $d_{yz}/d_{xy}$_$\pi_y^*$ to L(Py_$\pi^*$) | 36% |
| 4 | S46 | 24731 | 404 | 0.047 | **$d_{yz}/d_{xy}$_$\pi_y^*$ to $\pi_y^*$_$d_{yz}$** | 18% |
| 4 | S47 | 25076 | 399 | 0.007 | **$d_{yz}/d_{xy}$_$\pi_y^*$ to $\pi_y^*$_$d_{yz}$** | 41% |
| 5 | S63 | 27269 | 367 | 0.042 | L(Py_$\pi$) to L(Py_$\pi^*$)<br>$d_{yz}/d_{xy}$_$\pi_y^*$ to L(Py_$\pi^*$) | 37% |
| 5 | S67 | 28165 | 355 | 0.026 | L(amide_$p_y$) to L(Py_ $\pi^*$)<br>$d_{yz}/d_{xy}$_$\pi_y^*$ to $d_{z^2}$<br>$d_{yz}$_$\pi_y^*$ to L(Py_$\pi^*$) | 24%<br><br>11% |
| 5 | S68 | 28210 | 355 | 0.086 | $d_{yz}$_$\pi_y^*$ to L(Py_$\pi^*$) | 32% |
| 6 | S80 | 30759 | 325 | 0.016 | $d_{yz}$_$\pi_y^*$ to L(Py_$\pi^*$)<br>**$d_{yz}$_$\pi_y^*$ to $\pi_y^*$_$d_{yz}/d_{xy}$** | 25% |
| 6 | S86 | 31514 | 317 | 0.019 | L(amide_$p_z$) to $d_{z^2}$<br>**$d_{yz}$_$\pi_y^*$ to $\pi_y^*$_$d_{yz}$** | 17%<br>16% |
| 6 | S87 | 31804 | 314 | 0.010 | $d_{yz}$_$\pi_y^*$ to L(Py_$\pi^*$) | 42% |

[a] Py_$\pi^*$ = pyridine $\pi^*$ orbitals; amide_$p_n$ = amide nitrogen $p_y$ or $p_z$ orbitals

frequency) and stronger Mn−NO bond (higher $\nu$(Mn−NO) frequency) in **2**.

### C.3. TD-DFT Calculations and Spectral Assignments.

TD-DFT calculations were used to explore the nature of the lowest-lying excited states in **1** and **2** to assign their electronic spectra and to determine why these complexes can be photoactivated using visible light. BP86/TZVP was used for the TD-DFT calculations to predict the 90 lowest-lying excited states of $[Mn(PaPy_3(NO)]^+$ and $[Mn(PaPy_2Q)(NO)]^+$. Both of these complexes show overall similar results, so $[Mn(PaPy_3)(NO)]^+$ is discussed in the following. At this point the reader should be reminded that TD-DFT is generally not able to describe CT excited states well, and correspondingly, one has to be cautious when evaluating TD-DFT results. We therefore limit our analysis to a semiquantitative interpretation that is focused on the relative energies and intensities of different types of electronic transitions, but not so much on absolute values.

Table 4 lists selected TD-DFT calculated singlet excited states (oscillator strength, $f$(osc) > 0.006) for $[Mn(PaPy_3)(NO)]^+$. The absorption spectrum of complex **1** together with a Gaussian deconvolution of the experimental spectrum (bands A−J) is shown in Figure 7 (cf. Table 5), in comparison to the TD-DFT results. The main features in the calculated spectrum, labeled bands 1−6, are assigned as listed in Table 4. On the basis of the overall excellent agreement between the experiment and the calculations below 25000 $cm^{-1}$, the visible absorption spectrum of **1** can be assigned (cf. Table 5). The experimental bands A−C at 15641, 18626, and 20569 $cm^{-1}$, respectively, are associated with calculated bands 1 and 2 and are assigned to $d_{xy}$ to pyridine ($\pi^*$) metal-to-ligand (ML) CT transitions, $d_{xy}$ → L(Py_$\pi^*$), of the $PaPy_3^-$ ligand. The intense bands D, E, and F at higher energy between 22000−26000 $cm^{-1}$ correspond to the calculated features 3 and 4, which have again $t_{2g}$ → L(Py_$\pi^*$) character, but also show symmetry-allowed $d_\pi$_$\pi^*$(NO) → $\pi^*$(NO)_$d_\pi$ MLCT contributions (corresponding to the transitions between MOs ⟨109⟩ → ⟨115⟩; cf. Figure 6). Here, MO <109> corresponds to the antibonding combination between the $d_{yz}$_$\pi_y^*$ orbital and the amide $\pi$-donor orbital of the $PaPy_3^-$ ligand. Above 25000 $cm^{-1}$, the deviation between the experimental and the calculated UV−vis spectrum becomes quite pronounced. The intense, calculated feature 5, which is mostly of metal(d) → L(Py_$\pi^*$) MLCT and inner ligand ($PaPy_3^-$) character (cf. Table 4), has no equivalent feature at similar energy in the experimental data, and likely contributes to the intense features G and H. Finally, a main contribution to the symmetry-allowed $d_\pi$_$\pi^*$ → $\pi^*$_$d_\pi$ CT transition (corresponding to the transition between MOs ⟨106⟩ → ⟨115⟩; cf. Figure 6) is calculated at about 31000 $cm^{-1}$ (~325 nm), which is in fact quite similar to the analogous Ru(III) complex with NO (see Supporting Information, Figure S2), in addition to other Ru(III)-nitrosyls including $(NEt_4)_2[Ru(hybeb)(NO)]$.[53] In the case of **2**, stronger low-energy absorptions at 674 and 540 nm are observed, which are assigned to analogous $d_{xy}$ → L(Py/Q_$\pi^*$) transitions. Here, the presence of the Q group in the coligand that has a more extended $\pi$ system than Py leads to the increase in $\varepsilon$ in **2**.

Previously, it has been proposed that the photolability of ruthenium(III) complexes with NO arises from symmetry-allowed $d_\pi$_$\pi^*$ → $\pi^*$_$d_\pi$ CT transitions between the


dx.doi.org/10.1021/ic201967f | Inorg. Chem. 2011, 50, 12192−12203

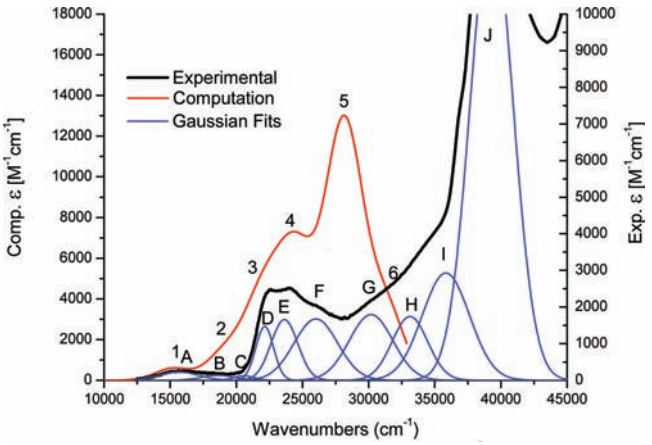


**Figure 7.** Experimental absorption spectrum of $[Mn(PaPy_3)(NO)]^+$ taken in MeCN solution at room temperature (black line, right vertical axis), including a Gaussian fit of the experimental data (blue lines). The resulting features A–J are listed in Table 5. The TD-DFT calculated spectrum (red line, left vertical axis) has six main features, labeled 1–6, as defined in Table 4. The calculated spectrum is cut off at about 32000 $cm^{-1}$ since only 90 excited states were calculated.

corresponding metal–NO bonding and antibonding MOs (red arrows in Figure 5).[54] Our results now show that the corresponding excited states for **1** and **2** are in fact located in the UV region, similar to $[Ru(PaPy_3)(NO)]^{2+}$, and therefore, the Mn-nitrosyls should be similar to the analogous Ru complexes and show photolabilization mostly in the UV range. The fact that some photolabilization of NO in complexes **1** and **2** is observed upon excitation in the 400–450 nm region can then be explained with the admixture of some $d_{\pi}\_\pi^* \rightarrow \pi^*\_d_{\pi}$ CT character into the metal(d) → L(Py_$\pi^*$) CT transitions that dominate this spectral region. This is different from $[Ru(PaPy_3)(NO)]^{2+}$, where no such admixture of $d_{\pi} \rightarrow \pi^*$(NO) CT character into the metal(d) → L(Py_$\pi^*$) CT transitions is observed in the visible region. However, these results can still not explain why the NO ligand in complexes **1** and **2** can be photolabilized with excitation wavelengths as low as 600 nm (**1**) and even 800 nm (**2**), where only $d_{xy}$ → L(Py/Q_$\pi^*$) transitions are observed. The photolabilization of NO at these low excitation energies must therefore be caused by other mechanisms than direct excitation of the $d_{\pi}\_\pi^* \rightarrow \pi^*\_d_{\pi}$ transitions. This aspect is further evaluated in the Discussion.

## D. DISCUSSION

In this paper, the spectroscopic properties and electronic structures of two analogous Mn(II) complexes with NO, $[Mn(PaPy_3)(NO)]^+$ (**1**) and $[Mn(PaPy_2Q)(NO)]^+$ (**2**), are analyzed, and based on the results, the nature of the Mn–NO bond in these complexes is characterized in detail. In addition, reasons for the photolability of the NO ligand upon vis–NIR excitation of these complexes are explored. Both **1** and **2** show similar geometric structures with short Mn–NO bond distances of 1.66–1.68 Å and close to linear Mn–N–O units. Vibrational spectroscopy further confirms the similarity in the properties of the Mn–NO units in these complexes, showing the diagnostic N–O stretch at 1733 and 1725 $cm^{-1}$ (from IR) in **1** and **2**, respectively. Using Raman spectroscopy, we were able to identify the Mn–NO stretch in **1** at 637 $cm^{-1}$, which shifts to 623 $cm^{-1}$ upon $^{15}N^{18}O$ labeling. These vibrational data provide key insight into the properties of the Mn–NO bond in these complexes. The observed $\nu$(N–O) values fall within the range of other diamagnetic manganese-nitrosyls (1700–1775 $cm^{-1}$; see Introduction),[24,25,55,56] but they are quite different from the N–O stretch in the paramagnetic [Mn(NO)(TC-5,5)] complex (1662 $cm^{-1}$).[18] This indicates that **1** and **2** have similar electronic structures as the other diamagnetic Mn(II)-nitrosyls, for example [Mn(TPP)(NO)], which have previously been described as Mn(I)–$NO^+$. In addition, the Mn–NO frequency of 637 $cm^{-1}$ is one of the highest transition-metal NO stretching frequencies reported to this date, which even supersedes $\nu$(Fe–NO) in ferric heme-nitrosyls (580–590 $cm^{-1}$)[22,49] and $\nu$(Ru–NO) in ruthenium(III) complexes with NO (~600 $cm^{-1}$).[37] This shows that the Mn–NO bond is very strong in the ground state of complexes **1** (and **2**), and hence the Mn–NO bond is likely very stable thermodynamically in these complexes (although there can be exceptions to this extrapolation because of low-lying excited states, see ref 49). DFT calculations are able to reproduce these geometric and spectroscopic properties well in the diamagnetic ($S = 0$) state of the complexes, whereas in the alternative triplet ground state, a distinct weakening of the Mn–NO bond is observed. This result along with the NMR data of the complexes clearly show that **1** and **2** indeed have diamagnetic ($S = 0$) ground states. The electronic structure of the complexes is best described as Mn(I)–$NO^+$, where Mn(I) is in the diamagnetic $[t_{2g}]^6$ low-spin state, and the $NO^+$ ligand forms two very strong $\pi$ backbonds with the $d_{xz}$ and $d_{yz}$ orbitals of the metal (where the Mn–N(O) bond corresponds to the $z$ axis). This explains the strong Mn–NO bonds observed in these complexes as reflected by their high Mn–NO stretching frequencies.

Importantly, the Mn(II) complexes with NO in their Mn(I)–$NO^+$ type ground states are isoelectronic to ferric heme-nitrosyls and Ru(III) complexes with NO, which can be best described as having the analogous Fe(II)/Ru(II)–$NO^+$ ground state electronic structures.[3,23,37,49,57–61] Note that all these compounds fall within the $\{M–NO\}^6$ category according to the Enemark–Feltham notation.[23] These iron- and ruthenium-nitrosyl complexes exhibit similar, short Fe/Ru–NO bond distances (~1.65 Å in the iron case),[3,62] linear Fe/Ru–N–O units as observed for **1** and **2**, and Fe/Ru–NO and N–O stretching frequencies in the 580–600 and ~1900 $cm^{-1}$ range, respectively.[16,22,49,52,63] In the case of $[Fe(PaPy_3)(NO)]^{2+}$ and $[Ru(PaPy_3)(NO)]^{2+}$, the N–O stretch is observed at 1919 and 1899 $cm^{-1}$, respectively.[17,18] Therefore,

**Table 5. Fit of the UV–vis Absorption Spectrum of $[Mn(PaPy_3)(NO)]^+$ (1)**

| band | position [$cm^{-1}$] (nm) | $\varepsilon$-coeff [$M^{-1}$ $cm^{-1}$] | assignment |
|---|---|---|---|
| A | 15641 (639) | 323 | |
| B | 18626 (537) | 190 | $d_{xy}$ to L(Py_$\pi^*$) |
| C | 20569 (486) | 170 | |
| D | 22142 (452) | 2099 | $d_{xy}$ to L(Py_$\pi^*$) |
| E | 23632 (423) | 2370 | $t_{2g}$ to L(Py_$\pi^*$) **$d_{yz}/d_{xy}\_\pi_y^*$ to $\pi_y^*\_d_{yz}$** |
| F | 26014 (384) | 2393 | $t_{2g}$ to L(Py_$\pi^*$) **$d_{yz}/d_{xy}\_\pi_y^*$ to $\pi_y^*\_d_{yz}$** |
| G | 30184 (331) | 2566 | $t_{2g}$ to L(Py_$\pi^*$) |
| H | 33118 (302) | 2488 | L(Py_$\pi$) to L(Py_$\pi^*$) **$d_{yz}\_\pi_y^*$ to $\pi_y^*\_d_{yz}$** |
| I | 35838 (279) | 4190 | |
| J | 39289 (255) | 17891 | |


dx.doi.org/10.1021/ic201967f | Inorg. Chem. 2011, 50, 12192–12203

relative to these analogous nitrosyls, complexes **1** and **2** exhibit *higher* metal−NO and *lower* N−O stretching frequencies as reported in this paper. This indirect correlation indicates a stronger $\pi$ backbond in complexes **1** and **2** compared to the isoelectronic iron- and ruthenium-nitrosyls. This is further confirmed by our DFT calculations, which show a distinct increase in the orbital mixing between the $d_{xz}/d_{yz}$ ($d_\pi$) orbitals of the metal and the $\pi^*$ orbitals of NO. For example, the corresponding antibonding combination, $d_{xz}\_\pi^*_x$, in complex **1** has 54% $\pi^*$ and 37% Mn character, compared to ∼70% $\pi^*$ and ∼25% metal contributions in the Fe/Ru-nitrosyls.[37,49] Therefore, the softer Mn(I) center forms the stronger $\pi$ backbond with the $\pi^*$ orbitals of $NO^+$ compared to the harder Fe(II) and Ru(II) centers, which explains the higher metal−NO and lower N−O stretching frequency in the manganese case; complexes **1** and **2** in fact have one of the strongest metal−$NO^+$ $\pi$ backbonds reported so far.

The Mn(I)−$NO^+$ electronic structure description implies that one-electron oxidation of complexes **1** and **2** should be metal centered, resulting in a Mn(II)−$NO^+$ species, since oxidation of the $NO^+$ ligand seems unlikely. In fact, complex **1** can be oxidized chemically (and electrochemically), and the resulting compound, $\mathbf{1}^{ox}$, exhibits an N−O stretching frequency of 1875 $cm^{-1}$, which is much higher than that of **1** (1733 $cm^{-1}$; see above). Interestingly, this number is very close to $\nu$(N−O) in the Fe/Ru(II)−$NO^+$ type complexes as discussed above. Hence, $\pi$-backbonding from the harder Mn(II) center in $\mathbf{1}^{ox}$ is reduced compared to **1** and is likely similar to Fe/Ru(II), and this accounts for the higher $\nu$(N−O) value of $\mathbf{1}^{ox}$.

The photolabilization of NO in simple Ru(III) complexes with NO, which is generally observed upon UV excitation of the complexes,[53,63−65] has been ascribed to the population of excited states with NO($\pi^*$) character,[16] and analogous observations are made here. The symmetry-allowed metal-to-ligand CT transitions within the Mn−N−O $\pi$ system, $d_{xz}\_\pi^*_x \rightarrow \pi^*_x\_d_{xz}$ (MOs ⟨107⟩ → ⟨113⟩) and $d_{yz}\_\pi^*_y \rightarrow \pi^*_y\_d_{yz}$ (MOs ⟨106⟩ → ⟨115⟩), generally labeled $d_\pi\_\pi^* \rightarrow \pi^*\_d_\pi$ in the following (see red arrows in Figure 5), are located in the UV region around 300 nm in both the Mn-nitrosyls **1** and **2**, and corresponding Ru-nitrosyl complexes (cf. Supporting Information, Figure S2). Excitation into these MLCT transitions effectively leads to the transfer of one electron from the metal back to the formally $NO^+$ ligand. This charge separation leads to excited states with effective Mn(II)−NO(radical) and Ru(III)−NO(radical) character, respectively. Because of the occupation of the metal−NO antibonding $\pi^*\_d_\pi$ orbitals (cf. Figure 6), the metal−NO bond is greatly weakened in these excited states (cf. also refs 16,66). Hence, the $d_\pi\_\pi^* \rightarrow \pi^*\_d_\pi$ MLCT excited states are ideally suited to promote photodissociation of NO in these complexes. This could further be promoted if the complexes could undergo an intersystem crossing into the corresponding $d_\pi\_\pi^* \rightarrow \pi^*\_d_\pi$ excited triplet states, which, because of their extended life times, are expected to be much more efficient in the photodissociation of NO.[63]

An additional difference between the Mn- and Ru-nitrosyls with the $PaPy_3^-$ and similar coligands is the fact that the ruthenium complexes generally show photolability upon UV excitation, whereas in **1** and **2**, NO can also be photodissociated upon excitation around 400−500 nm. The TD-DFT calculations presented in this paper are able to straightforwardly explain this difference. Whereas in the Ru(III) complexes with NO, the $d_\pi\_\pi^* \rightarrow \pi^*\_d_\pi$ MLCT transitions are generally only observed in the UV region as discussed above, the analogous Mn complexes **1** and **2** exhibit lower-energy electronic transitions around 400 nm that are of Mn($t_{2g}$) → L(Py_$\pi^*$) character and that contain significant $d_\pi\_\pi^* \rightarrow \pi^*\_d_\pi$ (MOs ⟨109⟩ → ⟨115⟩) MLCT contributions. No such transitions are observed in the analogous ruthenium complexes with the $PaPy_3^-$ and other similar coligands.[16] The presence of $d_\pi\_\pi^* \rightarrow \pi^*\_d_\pi$ excited states in the 400−500 nm spectral region of **1** (and **2**) is further substantiated by the observed strong resonance Raman enhancement of the Mn−NO stretch upon laser excitation in this energy region (cf. Figure 2). In fact, the strong resonance enhancement of this mode points toward an excited state that has a substantial displacement along the Mn−NO bond, in accordance with the proposed electron excitation into a Mn−NO antibonding orbital.

Direct excitation into the symmetry-allowed $d_\pi\_\pi^* \rightarrow \pi^*\_d_\pi$ MLCT transitions therefore explains the photolability of NO upon irradiation of complexes **1** and **2** in the 450 nm and the UV region (*direct mechanism*). In the case of Ru-nitrosyls, this mechanism is often limited to the UV region, which explains this apparent difference in the photochemistry of the analogous Mn(II) and Ru(III) complexes with NO. We believe that this difference relates to the fact that ruthenium (a) is a second row transition metal, and (b) carries a larger positive charge, which significantly increases the ligand field splitting in the ruthenium complexes, and hence, shifts all MLCT transitions to higher energy. However, photolabilization of NO via this direct mechanism is still not able to explain why complexes **1** and **2** can be photolyzed upon excitation in the vis−NIR region, where no $d_\pi\_\pi^* \rightarrow \pi^*\_d_\pi$ MLCT transitions occur according to the TD-DFT results.

Our spectroscopic results show that the Mn−N−O units in **1** and **2** have very similar properties, and correspondingly, should show quite similar energies for the $d_\pi\_\pi^* \rightarrow \pi^*\_d_\pi$ MLCT excited states. In contrast to this finding, NO photorelease in the vis−NIR region differs significantly between these two complexes: addition of the quinoline group to the ligand frame induces not only an increase in extinction coefficient of the low-energy $d_{xy}$ → L(Py/Q_$\pi^*$) bands and a small shift of these transitions to lower energy, but at the same time, greatly increases the quantum yield for NO release. This strong correlation between coligand properties and NO releasing properties of the complexes combined with the absence of $d_\pi\_\pi^* \rightarrow \pi^*\_d_\pi$ MLCT transitions in the vis−NIR region provides direct evidence that the photochemical mechanism of NO dissociation must be different in the vis−NIR region, and cannot correspond to the direct mechanism described above. We therefore propose that NO photorelease in the vis−NIR region is due to an *indirect mechanism*, where photoexcitation of the complexes first leads to occupation of a $d_{xy}$ → L(Py/Q_$\pi^*$) excited state, which then interconverts into a Mn(d) → NO($\pi^*$) excited state. The latter state has to correspond to a symmetry-forbidden (overlap-forbidden) MLCT, so no direct excitation into this Mn(d) → NO($\pi^*$) excited state is possible. There are two potential candidates for such symmetry-forbidden MLCTs: these could either be of symmetry-forbidden $d_\pi\_\pi^* \rightarrow \pi^*\_d_\pi$ character, which correspond to the $d_{xz}\_\pi^*_x \rightarrow \pi^*_y\_d_{yz}$ and $d_{yz}\_\pi^*_y \rightarrow \pi^*_x\_d_{xz}$ transitions, or of $d_{xy} \rightarrow \pi^*\_d_\pi$ (n → $\pi^*$) type. A closer inspection of the TD-DFT results for **1** shows that a multitude of excited states with distinct $d_{xy} \rightarrow \pi^*\_d_\pi$ MLCT character are in fact predicted in the vis−NIR region as shown in Table 6, which all have close to zero extinction coefficients because of the symmetry-forbidden


dx.doi.org/10.1021/ic201967f | Inorg. Chem. 2011, 50, 12192−12203

**Table 6. Electronic Transitions in $[Mn(PaPy_3(NO)]^+$ (1) with Significant $d_{xy} \rightarrow \pi^*\_d_\pi$ Character, Calculated with TD-DFT (BP86/TZVP)**

| TD-DFT State | energy [$cm^{-1}$] | energy [nm] | $f$(osc) | major contribution | percent contribution |
|---|---|---|---|---|---|
| **S1** | **13551** | **738** | **0** | **$d_{xy}$ to $\pi_x^*\_d_{xz}$** | **33%** |
| S5 | 14802 | 675 | 0 | $d_{xy}$ to $\pi_x^*\_d_{xz}$ | 9% |
| | | | | $d_{xy}$ to $\pi_y^*\_d_{yz}$ | 3% |
| S7 | 15657 | 639 | 0 | $d_{xy}$ to $\pi_y^*\_d_{yz}$ | 7% |
| S8 | 16181 | 618 | 0 | $d_{xy}$ to $\pi_y^*\_d_{yz}$ | 23% |
| S9 | 16687 | 599 | 0 | $d_{xy}$ to $\pi_y^*\_d_{yz}$ | 13% |
| S10 | 17849 | 560 | 0.0001 | $d_{xy}$ to $\pi_x^*\_d_{xz}$ | 47% |

nature of these transitions. *In particular, the lowest-energy excited singlet state is predicted to have significant $d_{xy} \rightarrow \pi^*\_d_\pi$ character.* Furthermore, intersystem crossing into the corresponding triplet states would be advantageous for NO photorelease because of the extended life times of triplet excited states (see above). We therefore propose the following model for the indirect mechanism of NO photolabilization of complexes **1** and **2** in the vis−NIR region: initial excitation of the complexes leads to the occupation of $d_{xy} \rightarrow$ L(Py/Q_$\pi^*$) excited states, which then interconvert into $d_{xy} \rightarrow \pi^*\_d_\pi$ excited states. These latter states are ideally set up to undergo intersystem crossing into the corresponding $d_{xy} \rightarrow \pi^*\_d_\pi$ triplet states, because of strong spin−orbit coupling between analogous $d_{xy} \rightarrow \pi^*\_d_\pi$ singlet and triplet excited states as shown in the Supporting Information. Here, intersystem crossing is promoted by the strong admixture of $d_\pi$ character into the unoccupied $\pi^*$ orbitals of $NO^+$. The $d_{xy} \rightarrow \pi^*\_d_\pi$ triplet states show a Mn(II)−NO(radical) type electronic structure where one electron has been transferred back to the $NO^+$ ligand, and the Mn−NO bond is weakened (because of occupation of an Mn−NO antibonding orbital). These excited states are therefore ideally suited for photorelease of NO (see above). The TD-DFT calculations further support these ideas and show that the lowest lying triplet state (T1) in fact has significant $d_{xy} \rightarrow \pi^*\_d_\pi$ CT character as shown in Table 7. We therefore propose that complexes **1** and **2** release NO from their T1 ($d_{xy} \rightarrow \pi^*\_d_\pi$) excited states. Figure 8 shows a summary of the properties of the lowest excited states of **1** that illustrates the indirect mechanism of NO photorelease. Once the molecule has entered a $d_{xy} \rightarrow \pi^*\_d_\pi$ excited triplet state, the Mn−NO antibonding nature of this state will promote ligand dissociation. Similar indirect mechanisms have also been demonstrated by rigorous TD-DFT calculations for the photodissociation of ligands in $[Ru(bpy)_2L_2]^{2+}$ complexes[67] and methylcobalamine.[68] Finally, the energies of the $d_{xy} \rightarrow \pi^*\_d_\pi$ excited triplet states show a small solvent dependency, and the corresponding excitation energies shift to lower frequencies in polar solvents like acetonitrile (see Supporting Information, Table S1).

This indirect mechanism by itself is not a new finding, but (a) somewhat resembles the established mechanism of action of organic triples sensitizers, although the actual details of the underlying process are different. In addition, (b) it has been known for a long time that many transition-metal complexes after initial excitation relax into excited states (by internal conversion and intersystem crossing) that are not *directly* accessible via light excitation, but which are active in ligand dissociation or chemical reactions.[69−73] However, up until now it was unclear if analogous mechanisms could be involved in the photodissociation of NO from transition-metal nitrosyls. Importantly, the identification of such an indirect mechanism in the light activation of manganese-nitrosyls as reported here opens up the door for a great tunability of the NO photorelease properties of the complexes with respect to two aspects:

(a) the better the energies of the initial $d_{xy} \rightarrow$ L(Py/Q_$\pi^*$) and the final $d_{xy} \rightarrow \pi^*$(NO)_$d_\pi$ excited triplet states are matched, the more efficient is the interconversion between these states, and hence, the higher the quantum yields for NO photorelease; and

(b) an increase in extinction coefficient in the vis−NIR region that leads to a larger number of molecules per second that are excited into the $d_{xy} \rightarrow$ L(Py/Q_$\pi^*$) state will likely lead to an increase in NO release.

**Table 7. First Seven Triple Excited States of $[Mn(PaPy_3(NO)]^+$ (1) with Significant $d_{xy} \rightarrow \pi^*\_d_\pi$ Character, Calculated with TD-DFT (BP86/TZVP)**

| TD-DFT State | energy [$cm^{-1}$] | energy [nm] | $f$(osc) | major contribution | percent contribution |
|---|---|---|---|---|---|
| **T1** | **134713** | **742** | **0** | **$d_{xy}$ to $\pi_x^*\_d_{xz}$** | **66%** |
| T2 | 13584 | 736 | 0 | $d_{xy}$ to $\pi_x^*\_d_{xz}$ | 1% |
| | | | | $d_{xy}$ to $\pi_y^*\_d_{yz}$ | 3% |
| T3 | 14377 | 696 | 0 | $d_{xy}$ to $\pi_x^*\_d_{xz}$ | 14% |
| T4 | 14739 | 679 | 0 | $d_{xy}$ to $\pi_x^*\_d_{xz}$ | 17% |
| | | | | $d_{xy}$ to $\pi_y^*\_d_{yz}$ | 6% |
| T5 | 15484 | 646 | 0 | $d_{xy}$ to $\pi_y^*\_d_{yz}$ | 13% |
| T6 | 16141 | 620 | 0 | $d_{xy}$ to $\pi_y^*\_d_{yz}$ | 48% |
| T7 | 16640 | 601 | 0 | $d_{xy}$ to $\pi_y^*\_d_{yz}$ | 25% |

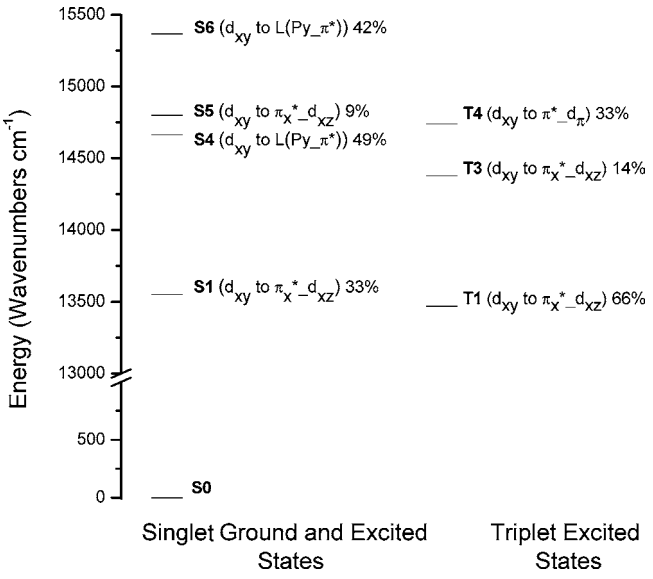


**Figure 8.** Selected singlet and triplet excited states of $[Mn(PaPy_3)(NO)]^+$ (**1**).


dx.doi.org/10.1021/ic201967f | *Inorg. Chem.* 2011, 50, 12192−12203

Both of these properties can be tuned via a variation in the coligand (here: $PaPy_3^-$ and $PaPy_2Q^-$). For example, coligands with even larger extinction coefficients in the NIR region should further enhance the NO photorelease properties. The critical $d_{xy} \rightarrow \pi^*\_d_\pi$ triplet excited state could be further lowered in energy by adding coligands with in-plane ($xy$) $\pi$-donor properties, enabling NO photorelease at even lower excitation energies. In addition, inner ligand $\pi \rightarrow \pi^*$ triplet excited states could in principle also be utilized to populate the key $d_{xy} \rightarrow \pi^*\_d_\pi$ triplet excited state required for photolabilization of NO. *Hence, the Mn(II) complexes with NO show the desired and long sought-after potential for easy tunability of their NO photolabilization properties*. This has been found difficult for compounds that operate via the direct mechanism (like Ru(III) complexes with NO), since the properties of the metal−$NO^+$ bond are much more difficult to vary to a greater extend compared to the properties of the coligand. On the other hand, the indirect mechanism does not seem to be operative for the Ru(III) complexes with NO, likely because of the stronger ligand field in this case that shifts the corresponding $d_{xy} \rightarrow \pi^*\_d_\pi$ MLCT excited states to higher energy, and hence, the $d_{xy} \rightarrow L(Py/Q\_\pi^*)$ and $d_{xy} \rightarrow \pi^*\_d_\pi$ MLCT excited singlet states are no longer in resonance for efficient interconversion.[74]

## ■ ASSOCIATED CONTENT

### Ⓢ Supporting Information

Excited states SOC derivation, and TD-DFT calculated absorption spectra of $[Mn(PaPy_3)(NO)]^+$ and $[Ru(PaPy_3)(NO)]^{2+}$. This material is available free of charge via the Internet at http://pubs.acs.org.

## ■ AUTHOR INFORMATION

### Corresponding Author

*E-mail: lehnertn@umich.edu (N.L.), pradip@chemistry.ucsc.edu (P.K.M.).

## ■ ACKNOWLEDGMENTS

This work was supported by a grant from 3M (NTFG # 5286067 to NL) and by the National Science Foundation (CHE-0957251 to P.M.). Mrs. U. Cornelissen (University of Kiel) is acknowledged for recording the FT-Raman spectrum of **1**.

## ■ REFERENCES

(1) Ignarro, L. J. *Nitric Oxide: Biology and Pathobiology*, 1st ed.; Academic Press: San Diego, 2000.
(2) Kalsner, S. *Nitric Oxide and Free Radicals in Peripheral Neurotransmission*; Birkhäuser: Boston, 2000.
(3) Lehnert, N.; Berto, T. C.; Galinato, M. G. I.; Goodrich, L. E. The Role of Heme-Nitrosyls in the Biosynthesis, Transport, Sensing, and Detoxificcation of Nitric Oxide(NO) in Biological Systems: Enzymes and Model Complexes. In *The Handbook of Porphyrin Science*; World Scientific: Singapore, 2011; Vol. *14*, Chapter 63, pp 1−247.
(4) Fang, F. C. *Nitric Oxide and Infection*; Kluwer Academic/Plenum Publishers: New York, 1999.
(5) Degoute, C. S. *Drugs* **2007**, *67*, 1053−1076.
(6) Moncada, S.; Higgs, E. A.; Bagetta, G. *Nitric Oxide and the Cell: Proliferation, Differentiation, and Death*; Princeton University Press: London, 1998.
(7) Kanwar, J. R.; Kanwar, R. K.; Burrow, H.; Baratchi, S. *Curr. Med. Chem.* **2009**, *16*, 2373−2394.
(8) Hirst, D.; Robson, T. *J. Pharm. Pharmacol.* **2007**, *59*, 3−13.
(9) Fry, N. L.; Mascharak, P. K. *Acc. Chem. Res.* **2011**, *44*, 289−298.
(10) Ford, P. C. *Acc. Chem. Res.* **2008**, *41*, 190−200.
(11) Rose, M. J.; Mascharak, P. K. *Curr. Opin. Chem. Biol.* **2008**, *12*, 238−244.
(12) Eroy-Reveles, A. A.; Mascharak, P. K. *Future Med. Chem.* **2009**, *1*, 1497−1507.
(13) Castano, A. P.; Mroz, P.; Hamblin, M. R. *Nat. Rev. Cancer* **2006**, *6*, 535−545.
(14) Detty, M. R.; Gibson, S. L.; Wagner, S. J. *J. Med. Chem.* **2004**, *47*, 3897−3915.
(15) Ford, P. C.; Bourassa, J.; Miranda, K.; Lee, B.; Lorkovic, I.; Boggs, S.; Kudo, S.; Laverman, L. *Coord. Chem. Rev.* **1998**, *171*, 185−202.
(16) Rose, M. J.; Mascharak, P. K. *Coord. Chem. Rev.* **2008**, *252*, 2093−2114.
(17) Patra, A. K.; Afshar, R.; Olmstead, M. M.; Mascharak, P. K. *Angew. Chem., Int. Ed.* **2002**, *41*, 2512−2515.
(18) Patra, A. K.; Mascharak, P. K. *Inorg. Chem.* **2003**, *42*, 7363−7365.
(19) Eroy-Reveles, A. A.; Hoffman-Luca, C. G.; Mascharak, P. K. *Dalton Trans.* **2007**, 5268−5274.
(20) Rose, M. J.; Olmstead, M. M.; Mascharak, P. K. *Polyhedron* **2007**, *26*, 4713−4718.
(21) Ghosh, K.; Eroy-Reveles, A. A.; Avila, B.; Holman, T. R.; Olmstead, M. M.; Mascharak, P. K. *Inorg. Chem.* **2004**, *43*, 2988−2997.
(22) Goodrich, L. E.; Paulat, F.; Praneeth, V. K. K.; Lehnert, N. *Inorg. Chem.* **2010**, *49*, 6293−6316.
(23) Enemark, J. H.; Feltham, R. D. *Coord. Chem. Rev.* **1974**, *13*, 339−406.
(24) Scheidt, W. R.; Hatano, K.; Rupprecht, G. A.; Piciulo, P. L. *Inorg. Chem.* **1979**, *18*, 292−299.
(25) Coleman, W. M.; Taylor, L. T. *J. Am. Chem. Soc.* **1978**, *100*, 1705−1710.
(26) Tangen, E.; Conradie, J.; Franz, K.; Friedle, S.; Telser, J.; Lippard, S. J.; Ghosh, A. *Inorg. Chem.* **2010**, *49*, 2701−2705.
(27) Franz, K. J.; Lippard, S. J. *J. Am. Chem. Soc.* **1998**, *120*, 9034−9040.
(28) Rowland, J. M.; Olmstead, M.; Mascharak, P. K. *Inorg. Chem.* **2001**, *40*, 2810−2817.
(29) Eroy-Reveles, A. A.; Leung, Y.; Beavers, C. M.; Olmstead, M. M.; Mascharak, P. K. *J. Am. Chem. Soc.* **2008**, *130*, 4447−4458.
(30) Perdew, J. P. *Phys. Rev. B* **1986**, *33*, 8822−8824.
(31) Becke, A. D. *J. Chem. Phys.* **1986**, *84*, 4524−4529.
(32) Schäfer, A.; Horn, H.; Ahlrichs, R. *J. Chem. Phys.* **1992**, *97*, 2571−2577.
(33) Schäfer, A.; Huber, C.; Ahlrichs, R. *J. Chem. Phys.* **1994**, *100*, 5829−5835.
(34) Frisch, M. J.; Trucks, G. W.; Schlegel, H. B.; Scuseria, G. E.; Robb, M. A.; Cheeseman, J. R.; Montgomery, J. A., Jr.; Vreven, T.; Kudin, K. N.; Burant, J. C.; Millam, J. M.; Iyengar, S. S.; Tomasi, J.; Barone, V.; Mennucci, B.; Cossi, M.; Scalmani, G.; Rega, N.; Petersson, G. A.; Nakatsuji, H.; Hada, M.; Ehara, M.; Toyota, K.; Fukuda, R.; Hasegawa, J.; Ishida, M.; Nakajima, T.; Honda, Y.; Kitao, O.; Nakai, H.; Klene, M.; Li, X.; Knox, J. E.; Hratchian, H. P.; Cross, J. B.; Adamo, C.; Jaramillo, J.; Gomperts, R.; Stratmann, R. E.; Yazyev, O.; Austin, A. J.; Cammi, R.; Pomelli, C.; Ochterski, J. W.; Ayala, P. Y.; Morokuma, K.; Voth, G. A.; Salvador, P.; Dannenberg, J. J.; Zakrzewski, V. G.; Dapprich, S.; Daniels, A. D.; Strain, M. C.; Farkas, O.; Malick, D. K.; Rabuck, A. D.; Raghavachari, K.; Foresman, J. B.; Ortiz, J. V.; Cui, Q.; Baboul, A. G.; Clifford, S.; Cioslowski, J.; Stefanov, B. B.; Liu, G.; Liashenko, A.; Piskorz, P.; Komaromi, I.; Martin, R. L.; Fox, D. J.; Keith, T.; Al-Laham, M. A.; Peng, C. Y.; Nanayakkara, A.; Challacombe, M.; Gill, P. M. W.; Johnson, B.; Chen, W.; Wong, M. W.; Gonzalez, C.; Pople, J. A. *Gaussian 03*; Gaussian, Inc.: Pittsburgh, PA, 2003.
(35) Neese, F. *ORCA*, Version 2.2; Max-Planck Institut für Bioanorganische Chemie: Mülheim/Ruhr, Germany, 2004.
(36) Hoffman-Luca, C. G.; Eroy-Reveles, A. A.; Alvarenga, J.; Mascharak, P. K. *Inorg. Chem.* **2009**, *48*, 9104−9111.

(37) Paulat, F.; Kuschel, T.; Nather, C.; Praneeth, V. K. K.; Sander, O.; Lehnert, N. *Inorg. Chem.* **2004**, *43*, 6979−6994.
(38) Albrecht, A. C. *J. Chem. Phys.* **1961**, *34*, 1476−1484.
(39) Spiro, T. G. In *Iron Porphyrins*; Lever, A. B. P., Gray, H. B., Eds.; *Addison-Wesley*: Reading, MA, **1983**; Part 2, pp 91−159.
(40) Krushinskii, L.; Shorygin, P. P. *Opt. Spectrosc.* **1961**, *11*, 12−17.
(41) Lehnert, N.; Ho, R. Y. N.; Que, L.; Solomon, E. I. *J. Am. Chem. Soc.* **2001**, *123*, 8271−8290.
(42) Parthasarathi, N.; Spiro, T. G. *Inorg. Chem.* **1987**, *26*, 2280−2282.
(43) Fujisawa, K.; Tateda, A.; Miyashita, Y.; Okamoto, K.; Paulat, F.; Praneeth, V. K. K.; Merkle, A.; Lehnert, N. *J. Am. Chem. Soc.* **2008**, *130*, 1205−1213.
(44) Paulat, F.; Lehnert, N. *Inorg. Chem.* **2007**, *46*, 1547−1549.
(45) Lehnert, N.; Sage, J. T.; Silvernail, N.; Scheidt, W. R.; Alp, E. E.; Sturhahn, W.; Zhao, J. *Inorg. Chem.* **2010**, *49*, 7197−7215.
(46) Lehnert, N.; Praneeth, V. K. K.; Paulat, F. *J. Comput. Chem.* **2006**, *27*, 1338−1351.
(47) Praneeth, V. K. K.; Nather, C.; Peters, G.; Lehnert, N. *Inorg. Chem.* **2006**, *45*, 2795−2811.
(48) Praneeth, V. K. K.; Neese, F.; Lehnert, N. *Inorg. Chem.* **2005**, *44*, 2570−2572.
(49) Praneeth, V. K. K.; Paulat, F.; Berto, T. C.; George, S. D.; Nather, C.; Sulok, C. D.; Lehnert, N. *J. Am. Chem. Soc.* **2008**, *130*, 15288−15303.
(50) Praneeth, V. K. K.; Haupt, E.; Lehnert, N. *J. Inorg. Biochem.* **2005**, *99*, 940−948.
(51) Berto, T. C.; Hoffman, M. B.; Murata, Y.; Landenberger, K. B.; Alp, E. E.; Zhao, J.; Lehnert, N. *J. Am. Chem. Soc.* **2011**, *133*, 16714−16717.
(52) Soldatova, A. V.; Ibrahim, M.; Olson, J. S.; Czernuszewicz, R. S.; Spiro, T. G. *J. Am. Chem. Soc.* **2010**, *132*, 4614−4625.
(53) Fry, N. L.; Rose, M. J.; Rogow, D. L.; Nyitray, C.; Kaur, M.; Mascharak, P. K. *Inorg. Chem.* **2010**, *49*, 1487−1495.
(54) Rose, M. J.; Mascharak, P. K. *Inorg. Chem.* **2009**, *48*, 6904−6917.
(55) Franceschi, F.; Hesschenbrouck, J.; Solari, E.; Floriani, C.; Re, N.; Rizzoli, C.; Chiesi-Villa, A. *J. Chem. Soc., Dalton Trans.* **2000**, 593−604.
(56) Lewis, J.; Irving, R. J.; Wilkinson, G. *J. Inorg. Nucl. Chem.* **1958**, *7*, 32−37.
(57) Bottomley, F. *Coord. Chem. Rev.* **1978**, *26*, 7−32.
(58) Bottomley, F. *Acc. Chem. Res.* **1978**, *11*, 158−163.
(59) Averill, B. A. *Chem. Rev.* **1996**, *96*, 2951−2964.
(60) Linder, D. P.; Rodgers, K. R.; Banister, J.; Wyllie, G. R. A.; Ellison, M. K.; Scheidt, W. R. *J. Am. Chem. Soc.* **2004**, *126*, 14136−14148.
(61) Roncaroli, F.; Videla, M.; Slep, L. D.; Olabe, J. A. *Coord. Chem. Rev.* **2007**, *251*, 1903−1930.
(62) Wyllie, G. R. A.; Scheidt, W. R. *Chem. Rev.* **2002**, *102*, 1067−1089.
(63) Tfouni, E.; Krieger, M.; McGarvey, B. R.; Franco, D. W. *Coord. Chem. Rev.* **2003**, *236*, 57−69.
(64) Works, C. F.; Jocher, C. J.; Bart, G. D.; Bu, X. H.; Ford, P. C. *Inorg. Chem.* **2002**, *41*, 3728−3739.
(65) Bordini, J.; Hughes, D. L.; Neto, J. D. D.; da Cunha, C. J. *Inorg. Chem.* **2002**, *41*, 5410−5416.
(66) Greene, S. N.; Richards, N. G. *Inorg. Chem.* **2004**, *43*, 7030−7041.
(67) Salassa, L.; Garino, C.; Salassa, G.; Gobetto, R.; Nervi, C. *J. Am. Chem. Soc.* **2008**, *130*, 9590−9597.
(68) Lodowski, P.; Jaworska, M.; Andruniow, T.; Kumar, M.; Kozlowski, P. M. *J. Phys. Chem. B* **2009**, *113*, 6898−6909.
(69) Adamson, A. W.; Waltz, W. L.; Zinato, E.; Watts, D. W.; Fleischauer, P. D.; Lindholm, R. D. *Chem. Rev.* **1968**, *68*, 541−585.
(70) Finkenzeller, W. J.; Thompson, M. E.; Yersin, H. *Chem. Phys. Lett.* **2007**, *444*, 273−279.
(71) Lamansky, S.; Djurovich, P.; Murphy, D.; Abdel-Razzaq, F.; Lee, H. E.; Adachi, C.; Burrows, P. E.; Forrest, S. R.; Thompson, M. E. *J. Am. Chem. Soc.* **2001**, *123*, 4304−4312.
(72) Nataraja., P.; Endicott, J. F. *J. Phys. Chem.* **1973**, *77*, 971−972.
(73) Crosby, G. A.; Alire, R. M.; Whan, R. E. *J. Chem. Phys.* **1961**, *34*, 743−748.
(74) The TD-DFT calculations on the analogous $[Ru(PaPy_3)(NO)]^{2+}$ complex provide some support for this idea, as in this case the lowest energy $d_{xy} \rightarrow \pi^*\_d_{\pi}$ singlet excited state is predicted to be ~5000 $cm^{-1}$ higher in energy compared to **1**.